Tetragonal SnOFeSe: A possible parent compound of the FeSe-based superconductor

Xiao-Xiao Man,[1] Pei-Han Sun,[1] Jian-Feng Zhang,[2] Zhong-Yi Lu,[1,*] and Kai Liu[1,†]

[1]*Department of Physics and Beijing Key Laboratory of Opto-Electronic Functional Materials and Micro-Nano Devices, Renmin University of China, Beijing 100872, China*

[2]*Institute of Physics, Chinese Academy of Sciences, Beijing 100190, China*

(Received 11 October 2022; revised 14 January 2023; accepted 19 January 2023; published 30 January 2023)

Recent experiments have reported that inserting metal atoms or small molecules in between the FeSe layers of β-FeSe can significantly enhance the superconducting transition temperature. Here, based on first-principles electronic structure calculations, we propose a stable compound SnOFeSe by alternatively stacking the SnO and β-FeSe layers. The predicted SnOFeSe has the same tetragonal structure as the well-known FeAs-based compound LaOFeAs, meanwhile their electronic structures in the nonmagnetic state are quite similar. The magnetic ground state of SnOFeSe is predicted to be the dimer antiferromagnetic (AFM) state, which is energetically only 2.77 (2.15) meV/Fe lower than the trimer (dimer-trimer-dimer-trimer) AFM state, indicating that strong magnetic fluctuations might be induced via slight modulation. Interestingly, SnOFeSe is at the verge of metal-insulator transition in these low-energy magnetic states, hence bridging the metallic parent compounds of iron-based superconductors and the insulating ones of cuprate superconductors. With the reduced dimensionality, monolayer SnOFeSe also shows great similarities in the electronic and magnetic properties to its bulk phase. Given that SnOFeSe is adjacent to magnetic frustration and resembles LaOFeAs in both crystal and electronic structures, we suggest that SnOFeSe is a possible superconductor parent compound, which may provide a promising platform to study the interplay between magnetism and unconventional superconductivity in FeSe-derived materials.

DOI: 10.1103/PhysRevB.107.045145

I. INTRODUCTION

Iron-based superconductors have inspired intensive interests both experimentally and theoretically since their discovery in 2008 [1–7]. With the simplest crystal structure among the iron-based superconductors ever found [1–7], the anti-PbO-type β-FeSe has become a prototypical system to study the physical properties of the iron-based superconductors. In addition, this system has attracted a lot of attention due to its unusual magnetic properties [2,8]. The superconducting transition temperature T_c of bulk β-FeSe is about 8 K at ambient pressure [2], and numerous works, therefore, have been devoted to improve the T_c via high pressure [9,10], chemical substitution [11], gate voltage [12], or epitaxial film growth [13]. In addition, intercalation of metal atoms or molecules into β-FeSe is another effective approach to enhance the superconductivity. For instance, metal-intercalated FeSe compounds, $A_xFe_{2-y}Se_2$ (A = Li, Na, K, Rb, Cs, Ca, Sr, Ba, Yb, Eu, Tl/K, or Tl/Rb), have shown the superconducting T_c's around 30 K [14–22]. With the intercalation of $Li_x(NH_2)_y(NH_3)_{1-y}$ [23], $(Li/Na)_x(NH_3)_y$ [24], $Li_x(C_5H_5N)_y$ [25], or $Li_{0.8}Fe_{0.2}OH$ [26,27] layers into β-FeSe, the T_c's can be significantly lifted above 40 K. The enhanced superconductivities in the FeSe-based compounds are believed to be intimately correlated with the modulation of electronic and magnetic properties of the FeSe layers.

We notice that the PbO-type SnO (space group: $P4/nmm$) has the same tetragonal structure as the anti-PbO-type β-FeSe [28–30] [Fig. 1(a)], although their metallic and nonmetallic elements are interchanged in atomic positions [28]. The experimental in-plane lattice constant of SnO ($a = 3.803$ Å) [28] matches quite well with that of β-FeSe ($a = 3.765$ Å) [2]. It is thus very likely to form the 1111-type FeSe-based compound SnOFeSe by alternatively stacking the SnO and FeSe layers [Fig. 1(d)], which is structurally identical to the FeAs-based compound LaOFeAs [1]. Since SnO is reported to be a semiconductor with an indirect band gap of 0.7 eV [31,32], the SnO layers can serve as insulating spacers in SnOFeSe and may make the FeSe layers more two dimensional (2D) in electronic behavior. In addition, SnOFeSe has the equal valence electrons as LaOFeAs, thus it may resemble the latter in electronic properties and might also become superconducting via appropriate modulation [1,5,33–37]. Based on these preliminary inferences, the physical properties of the 1111-type FeSe-based compound SnOFeSe deserve further in-depth theoretical investigation.

By using first-principles electronic structure calculations, here we propose a stable intercalation compound SnOFeSe formed by inserting SnO layers into β-FeSe, which is isostructural to the well-known LaOFeAs. We find that the electronic structure of SnOFeSe in the nonmagnetic (NM) state is quite similar to that of LaOFeAs. And we determine the magnetic ground state of SnOFeSe to be a dimer

*zlu@ruc.edu.cn
†kliu@ruc.edu.cn

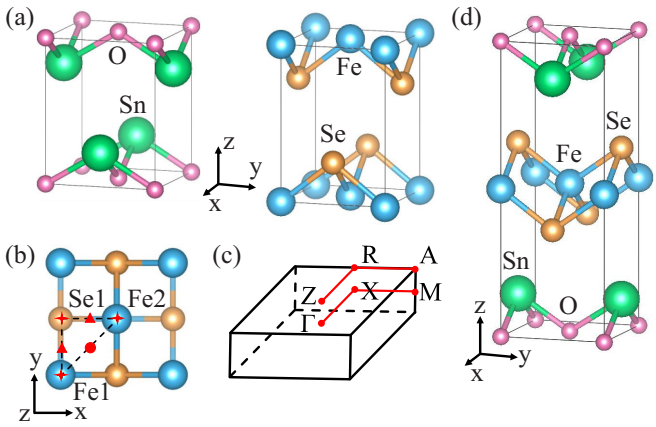

FIG. 1. (a) Crystal structures of the tetragonal-phase SnO and β-FeSe. (b) Six typical stacking sites of the SnO layer on top of the FeSe layer, labeled by the red crosses, dot, and triangles. (c) Brillouin zone (BZ) and (d) crystal structure of bulk SnOFeSe. The high-symmetry k points in the BZ are indicated by the red dots.

antiferromagnetic (AFM) state, in which the system is at the verge of metal-insulator transition. The monolayer SnOFeSe in the ultrathin limit has also been investigated in theory, which might be fabricated experimentally via epitaxial growth or mechanical exfoliation. Our calculation results suggest that SnOFeSe could be an ideal parent compound for studying the relationship between magnetism and unconventional superconductivity in FeSe-based superconductors.

II. COMPUTATIONAL DETAILS

To study the crystal structure, electronic structure, and magnetic properties of SnOFeSe, fully spin-polarized density functional theory (DFT) calculations were performed with the projector augmented wave method [38,39] as implemented in the Vienna *Ab Initio* Simulation Package (VASP) [40–42]. The generalized gradient approximation of the Perdew-Burke-Ernzerhof type [43] was adopted for the exchange-correlation functional. The kinetic energy cutoff of the plane-wave basis was set to 520 eV. The DFT-D2 method [44,45] was used to account for the van der Waals interaction in the layered materials [46]. The $16 \times 16 \times 8$, $4 \times 12 \times 8$, $3 \times 12 \times 8$, and $3 \times 12 \times 8$ Monkhorst-Pack **k**-point meshes were adopted to sample the Brillouin zones (BZs) of the unit cell and the $3\sqrt{2} \times \sqrt{2} \times 1$, $4\sqrt{2} \times \sqrt{2} \times 1$, and $5\sqrt{2} \times \sqrt{2} \times 1$ supercells for different magnetic states of bulk SnOFeSe, respectively. Meanwhile, for monolayer SnOFeSe, the **k**-point mesh along the $\mathbf{k}_z$ direction was adjusted to 1. The Fermi surface (FS) was broadened by the Gaussian smearing method with a width of 0.05 eV. The internal atomic positions and the cell parameters were fully optimized until the residual forces on all atoms were smaller than 0.01 eV/Å. The energy convergence criterion was set to 10^{-6} eV. For monolayer SnOFeSe, a vacuum layer larger than 20 Å was utilized to eliminate the interaction between image slabs along the (001) direction. The interlayer binding energy E_b of SnOFeSe was calculated according to the formula $E_b = E_{SnOFeSe} - E_{FeSe} - E_{SnO}$, where $E_{SnOFeSe}$ is the energy of SnOFeSe, and E_{FeSe} (E_{SnO}) is the energy of the FeSe (SnO) after removing the SnO (FeSe) layers from SnOFeSe. To check the dynamical stability, phonon spectra were calculated within the framework of density functional perturbation theory as implemented in the QUANTUM ESPRESSO package [47]. For the thermal stability, *ab initio* molecular dynamics simulations were carried out with the VASP package [40–42]. An *NVT* ensemble with a temperature T of 300 K controlled by the Nośe-Hoover thermostat was simulated. The total simulation time was set to 9 ps with a time step of 3 fs. In order to provide insight into the anisotropic property of SnOFeSe, the electrical conductivities along different directions were calculated within the constant-relaxation-time approximation of the Boltzmann transport equation using the BoltzTrap2 code [48,49].

III. RESULTS AND ANALYSIS

The crystal structures of the tetragonal-phase SnO and β-FeSe (space group: $P4/nmm$) are shown in Fig. 1(a). The experimental in-plane lattice constant of SnO is $a = 3.803$ Å [28], which is only 1.0% larger than that of β-FeSe ($a = 3.765$ Å) [2]. The rather small lattice mismatch between SnO and β-FeSe indicates that they might form the 1111-type FeSe-based compound SnOFeSe by alternatively intercalating the SnO and FeSe layers. In order to find out the most stable intercalation structure, we considered six nonequivalent stacking sites for the SnO layer on the FeSe plane [Fig. 1(b)], among which there are three top sites (Fe1 top, Fe2 top, and Se1 top) labeled by the red crosses, one hollow site labeled by the red dot, and two bridge sites (Fe1-Se1 bridge and Fe2-Se1 bridge) labeled by the red triangles. The concrete structures of SnOFeSe corresponding to the above stacking sites are displayed in Fig. S1 of the Supplemental Material (SM) [50]. After fully relaxing these structures in the NM state, we found that the energetically most stable one [Fig. 1(d)] has the same structure as the 1111-type FeAs-based compound LaOFeAs [1]. The calculated lattice constants of SnOFeSe are $a = b = 3.736$ Å and $c = 10.321$ Å, in which the in-plane lattice constant is quite close to those of pristine SnO and β-FeSe [2,28], suggesting the small strain effect after the intercalation. The BZ along with the high-symmetry k points of SnOFeSe are schematically displayed in Fig. 1(c).

We next examine the structural stabilities of SnOFeSe. The calculated phonon dispersion of SnOFeSe in the NM state along the high-symmetry paths of the BZ [Fig. 1(c)] is shown in Fig. 2(a), in which no imaginary phonon mode is observed. Considering that including AFM often improves the theoretical description on the phonons [46,51,52], we also calculated the phonon dispersion of SnOFeSe in the Néel state as displayed in Fig. S2 of the SM [50]. It can be seen that there is no imaginary phonon mode after considering the magnetism. The above phonon dispersion results indicate the dynamical stability of SnOFeSe. Furthermore, we carried out *ab initio* molecular dynamics simulations for the NM state of SnOFeSe, and obtained the time evolution of the free energy at 300 K as shown in Fig. S3(a) of the SM [50]. From a snapshot at 9 ps [Figs. S3(b) and S3(c) in the SM [50]], we can see that the structure remains intact without the bond breaking, suggesting that SnOFeSe is also stable at room temperature. In addition, we performed the convex hull calculations as shown in Fig. S4 of the SM [50], where

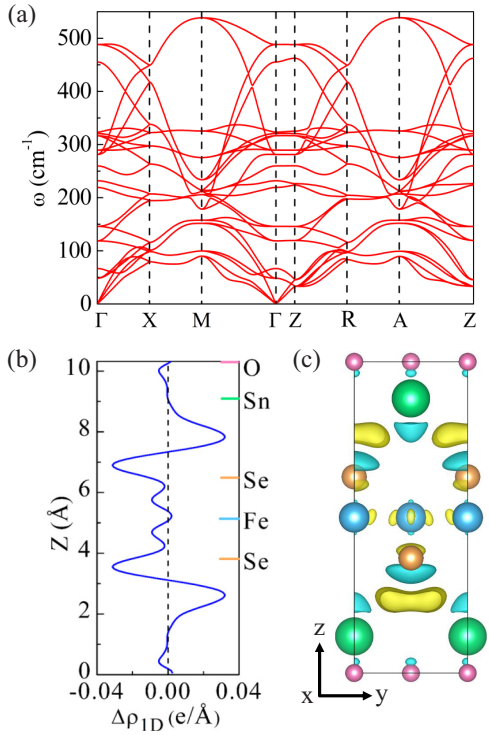

FIG. 2. (a) Phonon dispersion of bulk SnOFeSe in the NM state along the high-symmetry paths of the BZ [Fig. 1(c)]. (b) One-dimensional (1D) and (c) three-dimensional (3D) differential charge densities [$\Delta\rho = \rho_{\mathrm{SnOFeSe}} - \rho_{\mathrm{SnO}} - \rho_{\mathrm{FeSe}}$]. The atomic positions in panel (b) are marked by the color bars on the right axis. The yellow and cyan isosurfaces in panel (c) represent the electron accumulation and depletion areas, respectively. The isosurface value is set to 6.14×10^{-4} e/Å^3.

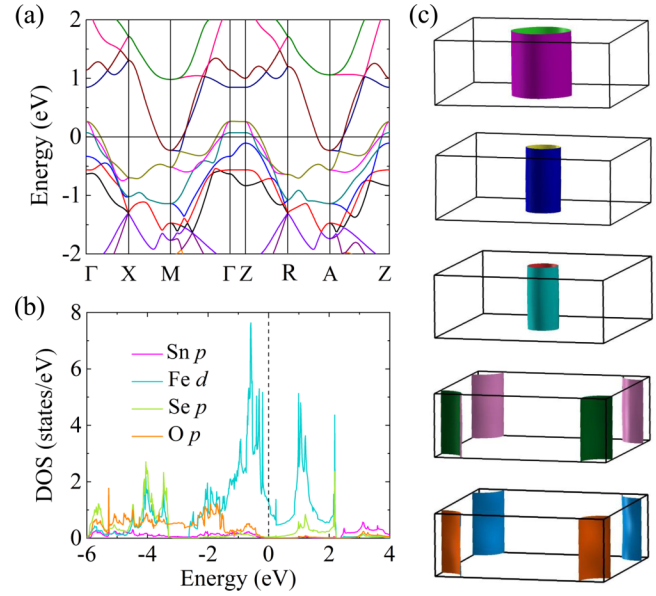

FIG. 3. (a) Band structure along the high-symmetry BZ paths, (b) PDOS, and (c) five Fermi surface sheets for bulk SnOFeSe in the NM state. The Fermi energy is set to zero.

the relative energy of SnOFeSe is 28.5 meV/atom above the convex hull of bulk SnO and β-FeSe. However, the interlayer binding energy of bulk (monolayer) SnOFeSe is calculated to be -112 (-44) meV/atom in the NM state, which is two to three times (comparable with) that of graphite [53–56]. To figure out the charge transfer between the SnO and FeSe layers in SnOFeSe, we then calculated the 1D and 3D differential charge densities as plotted in Figs. 2(b) and 2(c), respectively. It can be seen clearly that there are some electrons accumulated in the interlayer region. These calculation results show that SnOFeSe is a dynamically stable and thermodynamically metastable material that is very likely to be synthesized with a layer by layer approach by using the molecular beam epitaxial growth technique or the stacking method as other 2D heterostructures.

To investigate the electronic structure of SnOFeSe in the NM state, we calculated the band structure, the partial density of states (PDOS), as well as the FS. From the band structure shown in Fig. 3(a), we can see that there are five bands crossing the Fermi level, indicating a metallic behavior of SnOFeSe. The overall band characteristics look very similar to those of LaOFeAs [57,58] [Fig. S5(a) in the SM [50]], especially for the bands near the Fermi level. The calculated PDOS of SnOFeSe in Fig. 3(b) demonstrates that the Fe 3d orbitals contribute most in the energy range from -2 to 2 eV around the Fermi level, which is also similar to that of LaOFeAs [Fig. S5(b) in the SM [50]]. Figure 3(c) shows five FS sheets of SnOFeSe in the NM state, among which there are three hole-type pockets around the BZ center (Γ point) and two electron-type pockets around the BZ corner (M point). The perfect cylindrical shape of these FS sheets indicates the prominent 2D feature of SnOFeSe. Based on the information of FS, we then calculated the electron susceptibility $\chi(\mathbf{q})$. The real part $\chi'(\mathbf{q})$ shows a broad peak around the M point [Fig. 4(a)], suggesting the electronic instability of the NM state. Meanwhile, the imaginary part $\chi''(\mathbf{q})$ [Fig. 4(b)] also has considerable intensity around the M point, which reflects the FS nesting that can be discerned intuitively by shifting the Fermi pockets from Γ to M in Fig. 3(c). These results indicate that, besides the crystal structure [Fig. 1(d)], the electronic properties of SnOFeSe in the NM state also resemble those of LaOFeAs [59].

The existence of strong FS nesting in Fe-based superconductors may induce magnetic instabilities [60–64], thus we have further studied the magnetic properties of SnOFeSe. In addition to the aforementioned NM state, we have investigated

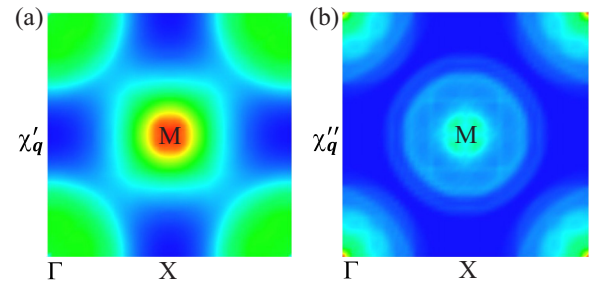

FIG. 4. (a) Real and (b) imaginary parts of the electron susceptibility χ plotted in the $q_z = 0$ plane for bulk SnOFeSe in the NM state.

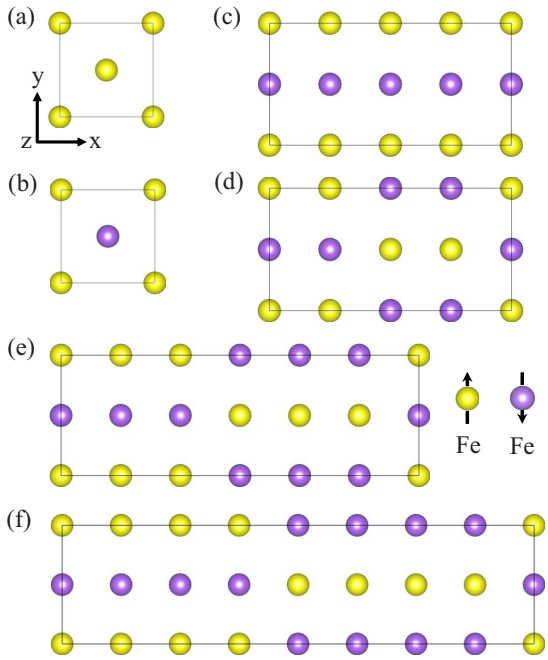

FIG. 5. Sketches of six typical spin configurations for the Fe lattice in SnOFeSe: (a) FM state, (b) checkerboard AFM Néel state, (c) single-stripe (collinear) AFM state, (d) dimer AFM state, (e) trimer AFM state, and (f) tetramer AFM state. Here, the solid rectangles represent the supercells, while the purple and yellow balls represent the spin-up and spin-down Fe atoms, respectively.

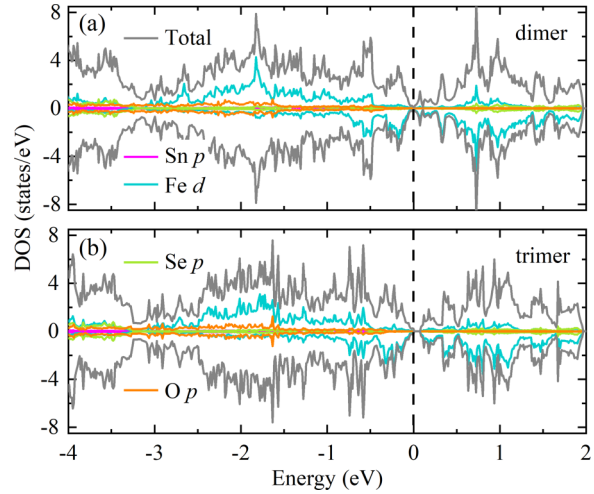

FIG. 6. Total DOS and PDOS for (a) the dimer AFM and (b) the trimer AFM states of bulk SnOFeSe. The Fermi energy is set to zero.

the ferromagnetic (FM) state and several typical AFM states including the checkerboard AFM Néel, stripe AFM, dimer AFM, trimer AFM, and tetramer AFM states, whose spin configurations are schematically shown in Fig. 5. The calculated relative energies of these magnetic states with respect to that of the NM state are listed in Table I. Clearly, the dimer AFM state possesses the lowest energy, being the magnetic ground state of SnOFeSe, which is similar to previous calculation results on β-FeSe [65]. It is worth noting that the energy of the trimer AFM state is quite close to and only 2.77 meV/Fe higher than that of the dimer AFM state. Inspired by our previous studies on β-FeSe [66], we also investigated the AFM state combined by Fe spin dimers and trimers, such as the dimer-trimer-dimer-trimer (di-tri-di-tri) AFM state, which is energetically between the dimer and trimer AFM states and only 2.15 meV/Fe higher than the former one (Table I). It turns out that with appropriate modulation there may exist magnetic fluctuations among these low-energy magnetic states (dimer, trimer, and their random combinations) [66]. Table I also lists the average local moments on Fe atoms for these magnetic states from our calculation, whose values are comparable to the calculated local moments in β-FeSe [67,68].

We next investigated the electronic structures of SnOFeSe in the above low-energy magnetic states. Figures 6(a) and 6(b) show the total and partial densities of states (DOSs) of SnOFeSe in the dimer and trimer AFM states, respectively. It can be seen that in these two AFM states the Fe $3d$ orbitals have the main contributions near the Fermi level. With a close inspection of the total DOS in the lowest-energy dimer AFM state, SnOFeSe shows a semimetal character with very low density of states at the Fermi level. In comparison, there is a rather small energy gap ($\approx$0.07 eV) for SnOFeSe in the trimer AFM state. These results demonstrate that SnOFeSe is at the verge of metal-insulator transition when the magnetism is taken into account.

In addition to the bulk phase, the monolayer form is also worth investigation for the layered materials. Likewise, we studied the dynamical stability as well as the electronic and magnetic properties of monolayer SnOFeSe. The calculated phonon dispersions of monolayer SnOFeSe in the NM and Néel states along the high-symmetry paths of the BZ are shown in Figs. S6 and S7 of the SM [50], respectively. A rather tiny imaginary frequency in the acoustic branch appears near the Γ point, which is common for the calculated phonon spectra of 2D materials [69–71]. It is not a sign of structure instability, but may originate from the difficulties in accurately calculating the rapid decaying interatomic forces [72]. The band structure and PDOS of monolayer SnOFeSe in the NM state are shown in Figs. 7(a) and 7(b), respectively.

TABLE I. Relative energies ΔE (in units of meV/Fe) of the FM, checkerboard AFM Néel, stripe AFM, dimer AFM, trimer AFM, tetramer AFM, and dimer-trimer-dimer-trimer (di-tri-di-tri) AFM states with respect to the NM state for bulk SnOFeSe. The corresponding average local moments $\overline{M}$ (in units of μ_B) on Fe atoms are also listed.

State	NM	FM	Néel	Stripe	Dimer	Trimer	Tetramer	di-tri-di-tri
ΔE	0.00	168.69	−33.15	−67.01	−86.34	−83.57	−77.31	−84.19
$\overline{M}$		2.34	1.75	1.94	2.04	2.02	1.99	2.01

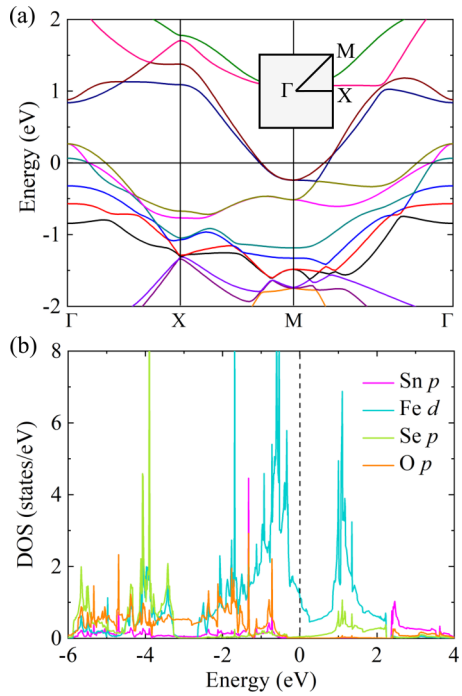

FIG. 7. (a) Band structure along the high-symmetry paths of the BZ and (b) PDOS for monolayer SnOFeSe in the NM state. The Fermi energy is set to zero.

The electronic band dispersion of monolayer SnOFeSe along the Γ-X-M-Γ path [Fig. 7(a)] is similar to that of the bulk phase [Fig. 3(a)], demonstrating the metallic behavior. Meanwhile, the DOS near the Fermi level is mainly contributed by Fe 3d orbitals [Fig. 7(b)]. We have further studied several typical spin configurations (Fig. 5) for monolayer SnOFeSe. After full relaxation, the FM state converges to the NM state, suggesting that the former is unstable. The calculated relative energies of the AFM magnetic states with respect to the NM state as well as the local moments on Fe atoms for monolayer SnOFeSe are listed in Table II. Like bulk SnOFeSe (Table I), the dimer AFM state is also the lowest-energy spin configuration for the monolayer form. Besides, the energy of the trimer (dimer-trimer-dimer-trimer) AFM state is merely 1.81 (0.74) meV/Fe higher than that of the dimer AFM state, suggesting that via slight tuning there may also exist magnetic frustration among the low-energy magnetic states in monolayer SnOFeSe. From the calculated total DOSs of the low-energy magnetic states (Fig. S8 in the SM [50]), we can see that in both the dimer and trimer AFM states monolayer SnOFeSe possesses tiny band gaps. Overall, the electronic and magnetic properties of monolayer SnOFeSe show great similarities to those of the bulk form.

IV. DISCUSSION AND SUMMARY

The SnOFeSe compound formed by intercalating the SnO layers into the anti-PbO-type β-FeSe has the following advantages. First, the same tetragonal symmetry and the small lattice mismatch between SnO and β-FeSe allow for an ideal intercalation without structural reconstruction and hence the formation of a stable crystal. Second, by comparing the calculated band structure, Fermi surface, and electrical conductivities of SnOFeSe in the NM state with those of bulk β-FeSe [73] (see the SM [50]), we find that the 2D characteristics of the electronic structure of bulk SnOFeSe are significantly enhanced. The improved two dimensionality due to the intercalation of insulating SnO layers facilitates the investigation of the intrinsic property of the FeSe layer. Third, SnOFeSe and β-FeSe show different magnetic behaviors and can thus be utilized for a comparative study. For β-FeSe, there is no long-range magnetic order at ambient pressure [74] and the AFM order only emerges under certain high pressures [10,75,76]. Our previous calculations indicated that there exist quasidegenerate AFM states with tiny energy difference of 0.3 meV/Fe in β-FeSe, which are responsible for the absence of magnetic order [66]. Here, the magnetic ground state (dimer AFM state) of SnOFeSe is energetically 2.77 meV/Fe lower than that of the trimer AFM state, providing an opportunity to detect the AFM order of the FeSe layer at low temperature and ambient pressure. Hence, SnOFeSe would be an interesting platform to study both electronic structure and magnetism of the quasi-2D FeSe layers.

As to the superconducting properties, SnOFeSe has the same crystal structure as the famous parent compound of the 1111-type Fe-based superconductor, namely, LaOFeAs. The electronic properties of SnOFeSe in the NM state, including band structure, density of states, and Fermi surface, are all similar to those of LaOFeAs. Moreover, both SnOFeSe and LaOFeAs have the AFM ground states, which are often in close proximity to the superconducting phase [77]. Since previous experiments have shown that doping elements (such as F, Sr, Pb, Th, Ca/F, and Ce/F) in LaOFeAs can suppress the AFM order and achieve the superconducting T_c's up to ≈30 K [1,5,33–37], we infer that the superconductivity in SnOFeSe can also be induced by appropriate modulations, such as element substitution [6,7,78], external pressure [79,80], ionic gating [12,27,81], etc.

In summary, by using first-principles electronic structure calculations, we have predicted a stable intercalation compound SnOFeSe that is isostructural to LaOFeAs, and have

TABLE II. Relative energies ΔE (in units of meV/Fe) of the magnetic states (AFM Néel, stripe AFM, dimer AFM, trimer AFM, tetramer AFM, and di-tri-di-tri AFM) with respect to the NM state for monolayer SnOFeSe. The corresponding average local moments $\overline{M}$ (in units of μ_B) on Fe atoms are also listed.

State	NM	Néel	Stripe	Dimer	Trimer	Tetramer	di-tri-di-tri
ΔE	0.00	−41.12	−73.39	−90.04	−88.23	−83.42	−89.30
$\overline{M}$		1.77	2.01	2.07	2.08	2.04	2.05

systematically investigated its electronic and magnetic properties. We find that the electronic structures of SnOFeSe in the NM state show great similarities with those of LaOFeAs. In addition, the magnetic ground state of SnOFeSe is the dimer AFM state, which is energetically only 2.77 (2.15) meV/Fe lower than the trimer (dimer-trimer-dimer-trimer) AFM state, indicating that strong magnetic fluctuations may emerge with fine tuning. In the low-energy magnetic states, SnOFeSe is on the verge of metal-insulator transition, which bridges the respective metallic and insulating parent compounds of iron-based and cuprate superconductors. Further calculations reveal that the electronic and magnetic properties of monolayer SnOFeSe in the ultrathin limit resemble those of its bulk phase. In consideration of the similarities between SnOFeSe and LaOFeAs, we suggest that SnOFeSe is a promising parent compound to explore the FeSe-based superconductivity, which calls for future experimental verification.

ACKNOWLEDGMENTS

We wish to thank J. G. Cheng, J. G. Guo, and X. L. Dong for helpful communications. This work was supported by the Beijing Natural Science Foundation (Grant No. Z200005), the National Natural Science Foundation of China (Grants No. 12174443 and No. 11934020), and the National Key R&D Program of China (Grants No. 2022YFA1403103 and No. 2019YFA0308603). Computational resources were provided by the Physical Laboratory of High Performance Computing at Renmin University of China.

[1] Y. Kamihara, T. Watanabe, M. Hirano, and H. Hosono, J. Am. Chem. Soc. **130**, 3296 (2008).
[2] F.-C. Hsu, J.-Y. Luo, K.-W. Yeh, T.-K. Chen, T.-W. Huang, P. M. Wu, Y.-C. Lee, Y.-L. Huang, Y.-Y. Chu, D.-C. Yan, and M.-K. Wu, Proc. Natl. Acad. Sci. USA **105**, 14262 (2008).
[3] X. C. Wang, Q. Q. Liu, Y. X. Lv, W. B. Gao, L. X. Yang, R. C. Yu, F. Y. Li, and C. Q. Jin, Solid State Commun. **148**, 538 (2008).
[4] M. Rotter, M. Tegel, and D. Johrendt, Phys. Rev. Lett. **101**, 107006 (2008).
[5] H. Takahashi, K. Igawa, K. Arii, Y. Kamihara, M. Hirano, and H. Hosono, Nature (London) **453**, 376 (2008).
[6] X. H. Chen, T. Wu, G. Wu, R. H. Liu, H. Chen, and D. F. Fang, Nature (London) **453**, 761 (2008).
[7] G. F. Chen, Z. Li, D. Wu, G. Li, W. Z. Hu, J. Dong, P. Zheng, J. L. Luo, and N. L. Wang, Phys. Rev. Lett. **100**, 247002 (2008).
[8] S.-B. Liu, S. Ma, Z.-S. Wang, W. Hu, Z.-A. Li, Q.-M. Liang, H. Wang, Y.-H. Zhang, Z.-Y.-W. Lu, J. Yuan, K. Jin, J.-Q. Li, L. Pi, L. Yu, F. Zhou, X.-L. Dong, and Z.-X. Zhao, Chin. Phys. Lett. **38**, 057401 (2021).
[9] Y. Mizuguchi, F. Tomioka, S. Tsuda, T. Yamaguchi, and Y. Takano, Appl. Phys. Lett. **93**, 152505 (2008).
[10] M. Bendele, A. Ichsanow, Y. Pashkevich, L. Keller, T. Strässle, A. Gusev, E. Pomjakushina, K. Conder, R. Khasanov, and H. Keller, Phys. Rev. B **85**, 064517 (2012).
[11] M. Abdel-Hafiez, Y.-Y. Zhang, Z.-Y. Cao, C.-G. Duan, G. Karapetrov, V. M. Pudalov, V. A. Vlasenko, A. V. Sadakov, D. A. Knyazev, T. A. Romanova, D. A. Chareev, O. S. Volkova, A. N. Vasiliev, and X.-J. Chen, Phys. Rev. B **91**, 165109 (2015).
[12] B. Lei, J. H. Cui, Z. J. Xiang, C. Shang, N. Z. Wang, G. J. Ye, X. G. Luo, T. Wu, Z. Sun, and X. H. Chen, Phys. Rev. Lett. **116**, 077002 (2016).
[13] Q.-Y. Wang, Z. Li, W.-H. Zhang, Z.-C. Zhang, J.-S. Zhang, W. Li, H. Ding, Y.-B. Ou, P. Deng, K. Chang, J. Wen, C.-L. Song, K. He, J.-F. Jia, S.-H. Ji, Y.-Y. Wang, L.-L. Wang, X. Chen, X.-C. Ma, and Q.-K. Xue, Chin. Phys. Lett. **29**, 037402 (2012).
[14] J. J. Ying, X. F. Wang, X. G. Luo, A. F. Wang, M. Zhang, Y. J. Yan, Z. J. Xiang, R. H. Liu, P. Cheng, G. J. Ye, and X. H. Chen, Phys. Rev. B **83**, 212502 (2011).
[15] J. G. Guo, S. F. Jin, G. Wang, S. C. Wang, K. X. Zhu, T. T. Zhou, M. He, and X. L. Chen, Phys. Rev. B **82**, 180520(R) (2010).
[16] A. Krzton-Maziopa, Z. Shermadini, E. Pomjakushina, V. Pomjakushin, M. Bendele, A. Amato, R. Khasanov, H. Luetkens, and K. Conder, J. Phys.: Condens. Matter **23**, 052203 (2011).
[17] L.-L. Sun, X.-J. Chen, J. Guo, P.-W. Gao, Q.-Z. Huang, H.-D. Wang, M.-H. Fang, X.-L. Chen, G.-F. Chen, Q. Wu, C. Zhang, D.-C. Gu, X.-L. Dong, L. Wang, K. Yang, A.-G. Li, X. Dai, H.-K. Mao, and Z.-X. Zhao, Nature (London) **483**, 67 (2012).
[18] A. F. Wang, J. J. Ying, Y. J. Yan, R. H. Liu, X. G. Luo, Z. Y. Li, X. F. Wang, M. Zhang, G. J. Ye, P. Cheng, Z. J. Xiang, and X. H. Chen, Phys. Rev. B **83**, 060512(R) (2011).
[19] C.-H. Li, B. Shen, F. Han, X. Y. Zhu, and H.-H. Wen, Phys. Rev. B **83**, 184521 (2011).
[20] M.-H. Fang, H.-D. Wang, C.-H. Dong, Z.-J. Li, C.-M. Feng, J. Chen, and H. Q. Yuan, Europhys. Lett. **94**, 27009 (2011).
[21] H.-D. Wang, C.-H. Dong, Z.-J. Li, Q.-H. Mao, S.-S. Zhu, C.-M. Feng, H. Q. Yuan, and M.-H. Fang, Europhys. Lett. **93**, 47004 (2011).
[22] T. P. Ying, X. L. Chen, G. Wang, S. F. Jin, T. T. Zhou, X. F. Lai, H. Zhang, and W. Y. Wang, Sci. Rep. **2**, 426 (2012).
[23] M. Burrard-Lucas, D. G. Free, S. J. Sedlmaier, J. D. Wright, S. J. Cassidy, Y. Hara, A. J. Corkett, T. Lancaster, P. J. Baker, S. J. Blundell, and S. J. Clarke, Nat. Mater. **12**, 15 (2013).
[24] H.-C. Lei, J.-G. Guo, F. Hayashi, and H. Hosono, Phys. Rev. B **90**, 214508 (2014).
[25] A. Krzton-Maziopa, E. V. Pomjakushina, V. Yu Pomjakushin, F. von Rohr, A. Schilling, and K. Conder, J. Phys.: Condens. Matter **24**, 382202 (2012).
[26] X. F. Lu, N. Z. Wang, H. Wu, Y. P. Wu, D. Zhao, X. Z. Zeng, X. G. Luo, T. Wu, W. Bao, G. H. Zhang, F. Q. Huang, Q. Z. Huang, and X. H. Chen, Nat. Mater. **14**, 325 (2015).
[27] B. Lei, Z. J. Xiang, X. F. Lu, N. Z. Wang, J. R. Chang, C. Shang, A. M. Zhang, Q. M. Zhang, X. G. Luo, T. Wu, Z. Sun, and X. H. Chen, Phys. Rev. B **93**, 060501(R) (2016).
[28] S.-X. Xu, Y.-T. Zou, J.-P. Sun, Z.-Y. Liu, X.-H. Yu, J. Gouchi, Y. Uwatoko, Z.-G. Cheng, B.-S. Wang, and J.-G. Cheng, Phys. Rev. B **101**, 104501 (2020).

[29] B. J. Pannetier and G. Denes, Acta Crystallogr. Sect. B **36**, 2763 (1980).

[30] E. Maskar, A. Fakhim Lamrani, M. Belaiche, A. Es-Smairi, D. P. Rai, and N. Fazouan, Superlattices Microstruct. **150**, 106776 (2021).

[31] Y. Ogo, H. Hiramatsu, K. Nomura, H. Yanagi, and T. Kamiya, Appl. Phys. Lett. **93**, 032113 (2008).

[32] K. M. Krishna, M. Sharon, M. K. Mishra, and V. R. Marathe, Electrochim. Acta **41**, 1999 (1996).

[33] H.-H. Wen, G. Mu, L. Fang, H. Yang, and X.-Y. Zhu, Europhys. Lett. **82**, 17009 (2008).

[34] K. Kaneyasu, R. Sakagami, M. Matoba, and Y. Kamihara, Jpn. J. Appl. Phys. **58**, 030911 (2019).

[35] G.-F. Chen, Z. Li, G. Li, J. Zhou, D. Wu, J. Dong, W.-Z. Hu, P. Zheng, Z.-J. Chen, H.-Q. Yuan, J. Singleton, J.-L. Luo, and N.-L. Wang, Phys. Rev. Lett. **101**, 057007 (2008).

[36] J. Prakash, S. J. Singh, S. Patnaik, and A. K. Ganguli, J. Phys.: Condens. Matter **21**, 175705 (2009).

[37] R.-C. Che, L. Wang, Z. Chen, C. Ma, C.-Y. Liang, J.-B. Lu, H.-L. Shi, H.-X. Yang, and J.-Q. Li, Europhys. Lett. **83**, 66005 (2008).

[38] G. Kresse and D. Joubert, Phys. Rev. B **59**, 1758 (1999).

[39] P. E. Blöchl, Phys. Rev. B **50**, 17953 (1994).

[40] G. Kresse and J. Furthmüller, Comput. Mater. Sci. **6**, 15 (1996).

[41] G. Kresse and J. Hafner, Phys. Rev. B **47**, 558 (1993).

[42] G. Kresse and J. Furthmüller, Phys. Rev. B **54**, 11169 (1996).

[43] J. P. Perdew, K. Burke, and M. Ernzerhof, Phys. Rev. Lett. **77**, 3865 (1996).

[44] X. Wu, M. C. Vargas, S. Nayak, V. Lotrich, and G. Scoles, J. Chem. Phys. **115**, 8748 (2001).

[45] S. Grimme, J. Comput. Chem. **27**, 1787 (2006).

[46] Q.-Q. Ye, K. Liu, and Z.-Y. Lu, Phys. Rev. B **88**, 205130 (2013).

[47] P. Giannozzi, S. Baroni, N. Bonini, M. Calandra, R. Car, C. Cavazzoni, D. Ceresoli, G. L. Chiarotti, M. Cococcioni, I. Dabo *et al.*, J. Phys.: Condens. Matter **21**, 395502 (2009).

[48] G. K. H. Madsen and D. J. Singh, Comput. Phys. Commun. **175**, 67 (2006).

[49] G. K. H. Madsen, J. Carrete, and M. J. Verstraete, Comput. Phys. Commun. **231**, 140 (2018).

[50] See Supplemental Material at http://link.aps.org/supplemental/10.1103/PhysRevB.107.045145 for six stacking structures of bulk SnOFeSe, phonon dispersion of bulk SnOFeSe in the Néel state, molecular dynamics simulations at 300 K, relative energies ΔE of $(SnO)_{n1}(FeSe)_{n2}$ with respect to those of bulk SnO and bulk β-FeSe, electronic structure of LaOFeAs, phonon dispersion of monolayer SnOFeSe, density of states for the low-energy magnetic states of monolayer SnOFeSe, electronic structure of bulk FeSe, electrical conductivities of bulk FeSe and bulk SnOFeSe, and the energies of different FeO and SnSe phases.

[51] M. P. Belov, A. B. Syzdykova, and I. A. Abrikosov, Phys. Rev. B **101**, 134303 (2020).

[52] P. V. S. Reddy, V. Kanchana, G. Vaitheeswaran, A. V. Ruban, and N. E. Christensen, J. Phys.: Condens. Matter **29**, 265801 (2017).

[53] L. A. Girifalco and R. A. Lad, J. Chem. Phys. **25**, 693 (1956).

[54] L. Spanu, S. Sorella, and G. Galli, Phys. Rev. Lett. **103**, 196401 (2009).

[55] Z. Liu, J. Z. Liu, Y. Cheng, Z.-H. Li, L. Wang, and Q.-S. Zheng, Phys. Rev. B **85**, 205418 (2012).

[56] X.-B. Chen, F.-Y. Tian, C. Persson, W.-H. Duan, and N.-X. Chen, Sci. Rep. **3**, 3046 (2013).

[57] F.-J. Ma and Z.-Y. Lu, Phys. Rev. B **78**, 033111 (2008).

[58] D. J. Singh and M.-H. Du, Phys. Rev. Lett. **100**, 237003 (2008).

[59] I. I. Mazin, D. J. Singh, M. D. Johannes, and M. H. Du, Phys. Rev. Lett. **101**, 057003 (2008).

[60] K. Kuroki, S. Onari, R. Arita, H. Usui, Y. Tanaka, H. Kontani, and H. Aoki, Phys. Rev. Lett. **101**, 087004 (2008).

[61] Y. M. Qiu, W. Bao, Y. Zhao, C. Broholm, V. Stanev, Z. Tesanovic, Y. C. Gasparovic, S. Chang, J. Hu, B. Qian, M. H. Fang, and Z. Q. Mao, Phys. Rev. Lett. **103**, 067008 (2009).

[62] A. Sekiyama, S. Kasai, M. Tsunekawa, Y. Ishida, M. Sing, A. Irizawa, A. Yamasaki, S. Imada, T. Muro, Y. Saitoh, Y. Ōnuki, T. Kimura, Y. Tokura, and S. Suga, Phys. Rev. B **70**, 060506(R) (2004).

[63] K. Kuroki, H. Usui, S. Onari, R. Arita, and H. Aoki, Phys. Rev. B **79**, 224511 (2009).

[64] Y. Sidis, M. Braden, P. Bourges, B. Hennion, S. NishiZaki, Y. Maeno, and Y. Mori, Phys. Rev. Lett. **83**, 3320 (1999).

[65] H.-Y. Cao, S.-Y. Chen, H.-J. Xiang, and X.-G. Gong, Phys. Rev. B **91**, 020504(R) (2015).

[66] K. Liu, Z.-Y. Lu, and T. Xiang, Phys. Rev. B **93**, 205154 (2016).

[67] K. Liu, B.-J. Zhang, and Z.-Y. Lu, Phys. Rev. B **91**, 045107 (2015).

[68] F.-J. Ma, W. Ji, J.-P. Hu, Z.-Y. Lu, and T. Xiang, Phys. Rev. Lett. **102**, 177003 (2009).

[69] M. Gao, Q.-Z. Li, X.-W. Yan, and J. Wang, Phys. Rev. B **95**, 024505 (2017).

[70] S. Cahangirov, M. Topsakal, E. Aktürk, H. Şahin, and S. Ciraci, Phys. Rev. Lett. **102**, 236804 (2009).

[71] C. Kamal and M. Ezawa, Phys. Rev. B **91**, 085423 (2015).

[72] H. Şahin, S. Cahangirov, M. Topsakal, E. Bekaroglu, E. Akturk, R. T. Senger, and S. Ciraci, Phys. Rev. B **80**, 155453 (2009).

[73] A. Subedi, L.-J. Zhang, D. J. Singh, and M.-H. Du, Phys. Rev. B **78**, 134514 (2008).

[74] T. M. McQueen, A. J. Williams, P. W. Stephens, J. Tao, Y. Zhu, V. Ksenofontov, F. Casper, C. Felser, and R. J. Cava, Phys. Rev. Lett. **103**, 057002 (2009).

[75] J.-P. Sun, B.-S. Wang, and J.-G. Cheng, Chinese Science Bulletin **62**, 3925 (2017).

[76] M. Bendele, A. Amato, K. Conder, M. Elender, H. Keller, H.-H. Klauss, H. Luetkens, E. Pomjakushina, A. Raselli, and R. Khasanov, Phys. Rev. Lett. **104**, 087003 (2010).

[77] C. de la Cruz, Q. Huang, J. W. Lynn, J.-Y. Li, W. R. II, J. L. Zarestky, H. A. Mook, G.-F. Chen, J.-L. Luo, N.-L. Wang, and P.-C. Dai, Nature (London) **453**, 899 (2008).

[78] J. Yang, X.-L. Shen, W. Lu, W. Yi, Z.-C. Li, Z.-A. Ren, G.-C. Che, X.-L. Dong, L.-L. Sun, F. Zhou, and Z.-X. Zhao, New J. Phys. **11**, 025005 (2009).

[79] L. Gao, Y.-Y. Xue, F. Chen, Q. Xiong, R.-L. Meng, D. Ramirez, C.-W. Chu, J. H. Eggert, and H. K. Mao, Phys. Rev. B **50**, 4260 (1994).

[80] C.-W. Chu, L. Gao, F. Chen, Z.-J. Huang, R.-L. Meng, and Y.-Y. Xue, Nature (London) **365**, 323 (1993).

[81] K. Taniguchi, A. Matsumoto, H. Shimotani, and H. Takagi, Appl. Phys. Lett. **101**, 042603 (2012).